⌘ *Author's Choice*

THE JOURNAL OF BIOLOGICAL CHEMISTRY VOL. 284, NO. 38, pp. 25938–25943, September 18, 2009

Fibulin 5 Forms a Compact Dimer in Physiological Solutions*[S]

Received for publication, April 22, 2009, and in revised form, July 9, 2009 Published, JBC Papers in Press, July 17, 2009, DOI 10.1074/jbc.M109.011627

Richard P. O. Jones[‡], Ming-Chuan Wang[§], Thomas A. Jowitt[§], Caroline Ridley[§], Kieran T. Mellody[§], Marjorie Howard[§], Tao Wang[‡], Paul N. Bishop[‡§], Andrew J. Lotery[¶], Cay M. Kielty[§], Clair Baldock[§], and Dorothy Trump[‡1]

From [‡]Genetic Medicine, Manchester Academic Health Science Centre, Faculty of Medical and Human Sciences, and the [§]Wellcome Trust Centre for Cell-Matrix Research, Faculty of Life Sciences, University of Manchester, Manchester M13 9PL and the [¶]Clinical Neurosciences Division, University of Southampton, Southampton SO17 1BJ, United Kingdom

Fibulin 5 is a 52-kDa calcium-binding epidermal growth factor (cbEGF)-rich extracellular matrix protein that is essential for the formation of elastic tissues. Missense mutations in fibulin 5 cause the elastin disorder cutis laxa and have been associated with age-related macular degeneration, a leading cause of blindness. We investigated the structure, hydrodynamics, and oligomerization of fibulin 5 using small angle x-ray scattering, EM, light scattering, circular dichroism, and sedimentation. Compact structures for the monomer were determined by small angle x-ray scattering and EM, and are supported by close agreement between the theoretical sedimentation of the structures and the experimental sedimentation of the monomer in solution. EM showed that monomers associate around a central cavity to form a dimer. Light scattering and equilibrium sedimentation demonstrated that the equilibrium between the monomer and the dimer is dependent upon NaCl and Ca^{2+} concentrations and that the dimer is dominant under physiological conditions. The dimerization of fragments containing just the cbEGF domains suggests that intermolecular interactions between cbEGFs cause dimerization of fibulin 5. It is possible that fibulin 5 functions as a dimer during elastinogenesis or that dimerization may provide a method for limiting interactions with binding partners such as tropoelastin.

Fibulins are a family of seven extracellular matrix glycoproteins, some of which associate with elastic fibers and basement membranes (1, 2). They are involved in the assembly, organization, and stabilization of macromolecular complexes (3). Fibulins contain arrays of cbEGF[2]-like domains and a fibulin-type C-terminal (Fc) module (4). Fibulins 3–5 have a modified N-terminal cbEGF domain, followed by five cbEGF domains (4).

Fibulin 5 (supplemental Fig. S1) is highly expressed in developing arteries with a low expression in adult vessels that is up-regulated following vascular injury and in atherosclerosis (5, 6). Expression has been detected in other elastin-rich tissues, including aorta, skin, uterus, lung, heart, ovary, and colon (5, 6). The extensibility of such tissues is provided by elastic fibers (7), and aging is associated with a loss of elasticity (8). Fibulin 5 is essential for elastinogenesis. The fibulin 5 knock-out mouse exhibits disorganized elastic fibers resulting in severe elastinopathies, with loose skin, vascular abnormalities, and emphysematous lungs. Similar changes are seen in an aged phenotype (9, 10). Mutations in fibulin 5 lead to the elastin disorder cutis laxa (11–13) and have been associated with age-related macular degeneration (14, 15).

It has been shown that fibulin 5 binds elastic fibers (16) and interacts with tropoelastin (10), fibrillin 1 (17), lysyl oxidase-like protein 1 (18), -2, and -4 (19), latent transforming growth factor-β-binding protein 2 (19), emilin 1 (20), apolipoprotein (a) (21), and superoxide dismutase (22). Through an RGD motif fibulin 5 interacts with integrins (6, 9, 23).

The assembly of elastic fibers is a complex hierarchical process. A model proposes that fibulin 5 associates with microfibrils via interactions with fibrillin 1; tropoelastin molecules bind fibulin 5 and coacervate, and lysyl oxidase-like protein 1 enzymes cross-link tropoelastin to form mature elastin (7, 16). Data that support this model indicate that fibulin 5 potentially increases the coacervation of tropoelastin, enhancing elastic fiber formation (24). However, other data suggest that fibulin 5 slows the maturation of elastin assemblies (25).

Rotary-shadowing EM has suggested that fibulin 5 exists as a short rod with a globular domain at one end (26). We used size-exclusion column multiangle laser light scattering (SEC-MALLS), small angle x-ray scattering (SAXS), EM single particle analysis, analytical ultracentrifugation (AUC), CD, and isoelectric focusing to investigate the structures of fibulin 5 in monomeric and dimeric form, and the equilibrium between the two forms.

EXPERIMENTAL PROCEDURES

Molecular Biology

The synthesis of the pCEP-His construct encoding full-length fibulin 5 was described previously (17). cDNAs encoding fragments of fibulin 5 and incorporating 5′ XhoI and 3′ NaeI restriction sites were obtained by PCR using the primers listed (supplemental Fig. S2). The restriction sites enabled directional in-frame subcloning of the cDNAs at the 3′ end of the 6-histidine tag coding

* This work was supported by Wellcome Trust Grants 123364 (to D. T., A. J. L., P. N. B., C. M. K., R. P. O. J., and C. R.), 072291 (to C. B. and M. C. W.), and VIP award (to R. P. O. J., and D. T.), and the National Institute for Health Research, Manchester Biomedical Research Centre.

⌘ *Author's Choice*—Final version full access.

[S] The on-line version of this article (available at http://www.jbc.org) contains supplemental Figs. 1–10 and additional references.

[1] To whom correspondence should be addressed: Genetic Medicine, University of Manchester, Manchester Academic Health Science Centre, St Mary's Hospital, Oxford Rd., Manchester M13 9WL, UK. Fax: 44-161-276-6606; E-mail: dorothy.trump@manchester.ac.uk.

[2] The abbreviations used are: cbEGF, calcium-binding epidermal growth factor; SAXS, small angle x-ray scattering; Fc, fibulin-type C-terminal; SEC-MALLS, size-exclusion column-multiangle laser light scattering; AUC, analytical ultracentrifugation; HOO, higher order oligomer; PSV, partial specific volume; AM/MM, average mass/monomer mass.

sequence in the pCEP-His vector. Correct in-frame transition and coding was confirmed by in-house DNA sequencing.

Purification of Recombinant Fibulin 5

Recombinant proteins were expressed by EBNA 293 cells stably transfected with pCEP-His constructs (17, 23) and secreted into serum-free medium (SAFC Biosciences). The polypeptides were purified by Ni^{2+}-affinity chromatography and applied to a Superdex 200 SEC (GE Healthcare). The following SEC buffers were used: buffer A, 50 mM Tris, pH 7.4, 0.5 M NaCl, 50 mM arginine, 50 mM glutamate (27), 5 mM EDTA, 5 mM EGTA; buffer B, 10 mM Tris, pH 7.4, 0.5 M NaCl, 2 mM EDTA, 2 mM EGTA; buffer C, 10 mM Tris, pH 7.4, 0.5 M NaCl; and buffer D, 10 mM Tris, pH 7.4, 0.5 M NaCl, 2 mM $CaCl_2$.

MALLS

The SEC eluate passed through an EOS 18-angle light scattering detector equipped with a 688 nm laser to determine masses, a quasi-elastic light scattering detector to determine hydrodynamic radii, and an r-EX refractometer to determine protein concentrations (all from Wyatt Technology Corp.).

EM Structures of Full-length Fibulin 5

EM structures were determined for monomeric fibulin 5 in the absence of Ca^2, and dimeric fibulin 5 in the presence of Ca^{2+}.

Grid Preparation—Carbon-coated 400-mesh copper grids underwent glow-discharge (EMITECH, mode K100X, 25 mA for 30 s) prior to the adsorption of fibulin 5 samples. The grids were negatively stained with 10 μl of 4% (w/v) uranyl acetate for 30 s and lightly blotted.

Microscopy—Images were obtained using a Tecnai 12 (120 keV) microscope (Philips) with a LaB6 filament. Images were recorded at 52,000 magnification by a CCD camera (Tietz Video and Image Processing Systems TemCam, resolution 2000 × 2000) using low electron doses (<10 e/Å^2) at the defocus value 2 μm. The final image pixel size was 1.9 Å.

Image Processing and Three-dimensional Reconstruction—The analysis of 6266 and 3052 single particles of size 19 and 22.8 nm^2 for the monomer and dimer, respectively, was performed using EMAN (28), Imagic 5 (29), and SPIDER software (30). Particles were aligned reference-free, and images were assigned to 120 and 80 classes that represented distinct views of the monomer and dimer, respectively. Preliminary three-dimensional structures were calculated by averaging the images in a class, using a Fourier common lines routine to determine the relative orientation of the classes, and then combining the classes. Assuming only c_1 symmetry, the structures were refined iteratively with 8 cycles of projection matching, and the convergence of the Fourier shell correlation coefficient was monitored. Application of the Fourier shell correlation coefficient = 0.5 criterion gave three-dimensional volume resolutions of 17 and 22 Å for the monomer and dimer, respectively.

SAXS Structure of Monomeric Full-length Fibulin 5

SAXS data were collected for fibulin 5 in the absence of Ca^{2+} (buffer A) on beamline X33 at the Deutsches Elektronen-Synchrotron (DESY, Hamburg, Germany) (31) using a 120-s exposure time and a 2.4-m sample detector distance to cover a momentum transfer interval 0.01 Å^{-1} < q < 0.5 Å^{-1} (where $q = 4\pi\sin\theta/\lambda$, where 2θ is the angle between the incident and scattered radiation). Buffer scattering intensities were subtracted from the sample scattering data. R_g and D_{max} values were evaluated with the indirect Fourier transform program Gnom (32). Particle shapes were restored *ab initio* based on the simulated annealing algorithm using Gasbor (33): Twenty runs generated similar shapes that were combined and filtered to produce an average model using the Damaver (34) software.

CD

Buffer-corrected CD spectra were measured between 190 and 260 nm by a J-810 spectropolarimeter (Jasco) using a 0.05-cm path length and an average of 10 scans. Spectra were deconvoluted by the Dichroweb (35) on-line server running the CDSSTR software (36) with reference set 7.

AUC of Full-length Fibulin 5

The Sednterp (37) software calculated buffer densities and viscosities, a mass of 49,779 Da, standard partial specific volume (PSV) of 0.7085 ml/g, and hydration of 0.3802 g (H_2O)/g (protein) for the recombinant fibulin 5 amino acid sequence. The MALLS-derived mass of 51,620 Da for the glycosylated fibulin 5 polypeptide and the estimate of 0.6170 ml/g for the PSV of carbohydrate (38) were used to calculate the estimate 0.7052 ml/g for the PSV for the glycosylated fibulin 5 polypeptide that was used in subsequent Sednterp (37) calculations. Sedimentation experiments were performed in an Optima XL-A analytical ultracentrifuge (Beckman Coulter) equipped with an absorbance optical system.

Sedimentation Velocity—Sample and buffer were centrifuged in a two-sector centerpiece in an An-60 Ti 4-hole rotor at 45,000 rpm at 20 °C. The sedimentation was monitored at 230 nm by 150 scans across a 1.4-cm radius with a step size of 0.003 cm. Sedfit (39) performed Lamm equation boundary modeling to calculate size $c(s)$ and mass $c(M)$ distributions. Sednterp (37) used S values for $c(s)$ maxima to calculate standard sedimentation coefficient $s_{20,w}$ values and hydrodynamic radii R_H values.

Sedimentation Equilibrium—Sedimentation equilibrium experiments determined the [NaCl] dependence of the AM/MM ratio and the dimer dissociation constant K_d in the absence of Ca^{2+} and the [Ca^{2+}] dependence of AM/MM and K_d for fibulin 5 in 150 mM NaCl. Each six-sector centerpiece contained solutions with only one cation concentration combination but three protein concentrations at 0.4, 2.4, and 2.5 μM corresponding to absorbances at 230 nm of ~ 0.5, 1, and 2, respectively; protein-free reference solutions of the same cation composition occupied the remaining three spaces in each centerpiece. The centerpieces were centrifuged in an An-50 Ti 8-hole rotor at 4 °C at sequential speeds 8000, 15,000, and 20,000 rpm. At each speed, 14 h allowed the sedimentation to reach equilibrium before data were collected. Twenty replicate scans with the maximum radial resolution of 0.001 cm were acquired at wavelengths 230, 235, and 280 nm. Global data analysis was performed by the Sedphat software (40).

RESULTS

Purification and Glycosylation of Fibulin 5 Polypeptides—Full-length fibulin 5 (residues 27–448), and the fragments of

TABLE 1

Hydrodynamic parameters for full-length fibulin 5 monomers, dimers, and HOOs were determined from the analysis of solution (sol)(MALLS, AUC, and SAXS) and EM data as indicated

D_{max} is the maximum dimension. The means and standard errors shown were calculated from results for three batches of protein.

Ca^{2+}	Fibulin 5 oligomer	Mass	f/f_0[a]	f/f_0[b]	$s_{20,w}$ ($\times 10^{13}$ S)	R_H	D_{max}
		kDa				*nm*	*nm*
Absent	^{sol}monomer	51.6 ± 0.4[c]	1.46 ± 0.05	1.48 ± 0.01	3.73 ± 0.02[b]	3.61 ± 0.02[b]	
	^{SAXS}monomer	51.6[d]			3.80[e]	3.54[e]	13[e]
	^{EM}monomer				3.79[f]	3.55[f]	10[f]
Present	^{sol}monomer	51.6[d]		1.55 ± 0.07	3.6 ± 0.2[b]	3.8 ± 0.2[b]	
	^{sol}dimer	103.2[d]	1.3 ± 0.1	1.64 ± 0.07	5.3 ± 0.2[b]	5.0 ± 0.2[b]	
	^{EM}dimer				5.31[f]	5.07[f]	15[f]
	^{sol}HOOs	200–1000[c]					
		<1000[g]	1.48				

[a] Sedfit (39) determined the best fit for mass-independent frictional ratio f/f_0.
[b] Sednterp (37) used the MALLS-derived mass and the S values for $c(s)$ maxima to calculate f/f_0, standard sedimentation coefficient $s_{20,w}$ and hydrodynamic radius R_H.
[c] Mass was derived from MALLS.
[d] Mass was calculated from the MALLS-derived mass of the monomer.
[e] Hydropro (43) calculated theoretical standard hydrodynamic parameters for the SAXS monomer structure.
[f] Hydromic (42) calculated theoretical standard hydrodynamic parameters for the EM structures.
[g] Mass range was estimated from the c(*M*) distribution (S7B), which depends upon f/f_0.

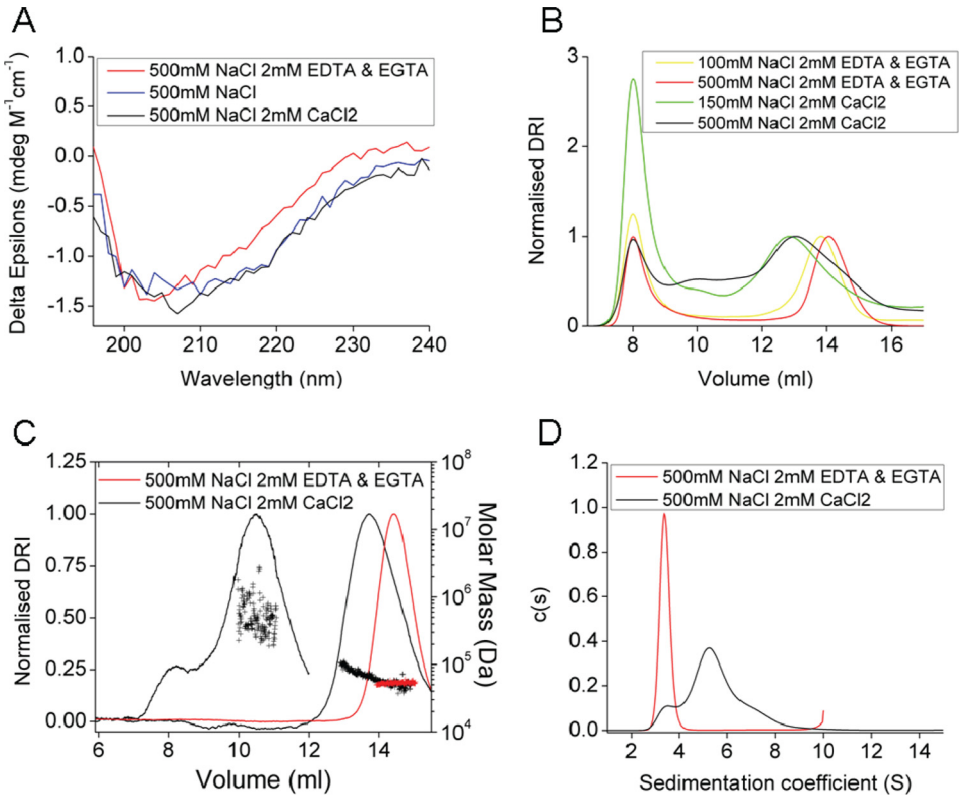

FIGURE 1. **CD, SEC-MALLS, and velocity sedimentation for full-length fibulin 5.** *A,* mean CD spectra for three batches of fibulin 5 purified by SEC in each buffer. *B* and *C,* chromatograms show the dependence of the differential refractive index (*DRI*) upon [NaCl] and [Ca^{2+}]. The DRI was normalized to 1.0 for each peak maximum; the column void positions were co-registered at 8 ml. *B,* first applications of fibulin 5 to the SEC. *C,* selected fractions were reapplied to SEC-MALLS to determine molar masses. *D,* sedimentation of SEC-purified fractions of fibulin 5 in the absence (*red line*, monomer) and presence (*black line*, mainly dimer) of Ca^{2+}. $c(s)$ size distributions were calculated by Sedfit (39).

fibulin 5 that included residues 26–333 (cbEGF-like domains 1–6), 120–333 and 127–333 (cbEGFs 2–6), 127–287 (cbEGFs 2–5), and 342–448 (the Fc domain) were purified from media to homogeneity by Ni^{2+}-affinity chromatography. The purified polypeptides were applied to SDS-PAGE followed by staining with Coomassie Blue (supplemental Fig. S3*A*). Amounts of the fragment comprising residues 342–448 were insufficient to be detected by Coomassie staining of acrylamide gels following Ni^{2+}-affinity purification and were later shown to elute at the void of the SEC in buffer C, suggesting aggregation (supplemental Fig. S3*D*). This fragment was not investigated further.

Fibulin 5 contains two potential *N*-linked glycosylation sites at residues 283 and 296 in cbEGF 5 and cbEGF 6, respectively. The glycosylation of recombinant fibulins has been demonstrated previously (26). A Western blot following treatment with (+) or without (−) *N*-glycosidase (supplemental Fig. S3*B*) showed that the EBNA 293 cells glycosylated the full-length polypeptide and fragments 26–333 and 120–333. The MALLS-derived masses for all polypeptides that contained one or more glycosylation sites were larger than those calculated by Sednterp (37) from the primary amino acid sequences (Table 1 and supplemental Fig. S4).

Folding—CD spectra were measured for the cbEGF-containing fragments in buffer C and for full-length fibulin 5 in three buffers (B–D) to determine the Ca^{2+} dependence of folding. The CD spectra (Fig. 1*A* and supplemental Fig. S5*A*) show that all of the polypeptides are folded in all of the buffers and display minima at ~205 nm between characteristic minima at 198 nm for unordered structure and at 216 nm for β-strand (41). Deconvolution of the spectra by CDSSTR software (36) provided estimates of secondary structure content (supplemental Fig. S6) that ranked unordered > strand > turn > helix. The high unordered contents may reflect that cbEGFs are small, tightly folded domains locked by internal disulfide bonds without extended regions of "conventional" secondary structures. A Student's *t* test (4

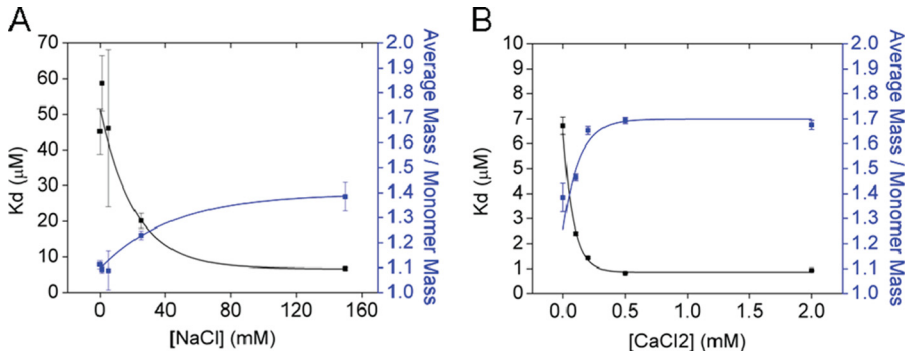

FIGURE 2. **Equilibrium sedimentation of full-length fibulin 5.** *A,* in the absence of Ca^{2+} equilibrium sedimentation established the [NaCl] dependence of the dimer dissociation constant K_d and the ratio AM/MM. *B,* [Ca^{2+}] dependence of K_d and AM/MM was determined for fibulin 5 in 150 mM NaCl. Data were analyzed by global nonlinear regression within Sedphat (40): Each *error bar* was determined by 100 Monte-Carlo simulations of the experimental data.

degrees of freedom, $p < 0.05$) showed the fits (indicated by normalized root mean square deviation (35)) of the CD spectra for full-length fibulin 5 were worse when Ca^{2+} was present. This may reflect the Ca^{2+}-induced "setting" of the cbEGFs into a more rigid structure with less well modeled secondary structure. However, statistically significant differences in secondary structure contents for full-length fibulin 5 in different buffers were not detected.

Ca^{2+}-dependent Oligomerization—The full-length fibulin 5 polypeptide was analyzed by size-exclusion chromatography in four different buffers (Fig. 1*B*). In the absence of Ca^{2+} there was a peak at 14 ml and a second peak at the void volume (8 ml) that was assumed to be aggregate. The presence of 2 mM Ca^{2+} caused a left shift of the main peak to 13 ml, the appearance of a continuum, and a second maximum at 10 ml. Increasing the salt concentration to 500 mM decreased the amount of aggregate in the void volume, and so 500 mM salt buffers were used for subsequent MALLS, CD, and sedimentation velocity experiments.

Chromatograms (Fig. 1*C*) show the reapplication of selected SEC fractions to the SEC equilibrated in the same buffer so that molar masses could be determined from the MALLS data in the absence of base-line interference from the column-void peak. In the absence of Ca^{2+} (buffer B), the reapplication to the SEC of the elution fraction 14–14.5 ml (*red line,* Fig. 1*B*) produced a single peak centered at 14.4 ml (*red line,* Fig. 1*C*) due entirely to monomeric fibulin 5, as shown by the flat trace of calculated masses (*red crosses,* Fig. 1*C*). The mean of average masses determined for three batches of monomer 51.6 ± 0.4 kDa enabled the calculation of a modified PSV (38) for the glycosylated full-length polypeptide that was used in the AUC analyses. In the presence of Ca^{2+} (buffer D), the reapplication to the SEC of the elution fraction 13–13.5 ml (*black line,* Fig. 1*B*) gave a broader peak centered at 13.7 ml that contained both monomeric and dimeric forms (*black line,* Fig. 1*C*). The SEC fraction 13–13.5 ml containing mainly the dimeric form was run on SDS-PAGE under both reducing and nonreducing conditions, and a Western blot (supplemental Fig. S3*C*) showed that dimerization is not mediated by intermolecular disulfide bonds. This suggests, as expected, that all cysteines are involved in intramolecular disulfide bonds that stabilize a correctly folded structure. Also in the presence of Ca^{2+} (buffer D), the reapplication to the SEC of the elution fraction 10–10.5 ml (*black line,* Fig. 1*B*) gave a peak centered at 10.5 ml (*black line,* Fig. 1*C*) with the estimated mass range 200–1000 kDa. This peak includes higher order oligomers (HOOs) estimated to range from a tetramer to a 20-mer.

Selected fractions collected during the first SEC runs in the presence (buffer D) and absence (buffer B) of Ca^{2+} underwent velocity sedimentation, and (mass-independent) frictional ratios (f/f_0) (Table 1) and hence $c(s)$ distributions (Fig. 1*D*) were calculated by Sedfit (39). In the absence of Ca^{2+}, the $c(s)$ had a maximum at 3.36 S that was assigned as monomer. In the presence of Ca^{2+}, the $c(s)$ was dominated by a maximum at 5.2 S that was assigned as a dimer, although small amounts of monomer and possibly trimer were also visible. Sednterp (37) used the MALLS-derived masses and the S values for $c(s)$ maxima to calculate f/f_0, $s_{20,w}$, and R_H values (Table 1). For the monomer in the absence of Ca^{2+}, agreement between the mass-dependent f/f_0 calculated by Sednterp (37) and the mass-independent f/f_0 calculated by Sedfit (39) provided confidence that both the MALLS-derived mass and the $c(s)$ peak assignment are correct. Statistically significant differences between $s_{20,w}$ and R_H values for the monomer in the presence and absence of Ca^{2+} were not detected. This suggests that any shape change is subtle.

The SEC fraction 10–10.5 ml (*black line,* Fig. 1*B*) containing fibulin 5 HOOs in the presence of Ca^{2+} (buffer D) was subjected to velocity sedimentation, and Sedfit (39) calculated the $c(s,^*)$ distribution, which is independent of both masses and f/f_0 values, and floated the f/f_0 to obtain the $c(s)$ distribution, which follows closely the $c(s,^*)$ distribution (supplemental Fig. S7*A*). It is intriguing that the f/f_0, a weighted average for the HOOs, is similar to those measured for the monomer (Table 1). This suggests that the shapes of the HOOs are not linear. Sedfit (39) converted the $c(s)$ distribution into the $c(M)$ distribution for the HOOs (supplemental Fig. S7*B*). The $c(M)$ cut-off at ~1000 kDa is consistent with the MALLS cut-off (Table 1).

Chromatograms (supplemental Fig. S5*B*) for first applications to the SEC equilibrated in buffer C show the oligomerization of fragments that contain only cbEGF domains. MALLS-derived masses for the fragment that includes residues 120–333 show that the peak at 14.9 ml is because of monomers, and the peak at 13.5 ml is because of dimers (supplemental Fig. S5*C*).

Sedimentation equilibrium experiments determined the dependence of the equilibrium between the monomer and the dimer upon [NaCl] and [Ca^{2+}]. In the absence of calcium, increasing the [NaCl] to 150 mM produced an exponential growth of AM/MM, accompanied by an exponential decay in K_d (Fig. 2*A* and supplemental Fig. S8). An explanation is that salt overcomes the electrostatic repulsion between monomers. The isoelectric point of 4.73 measured for glycosylated full-length fibulin 5 (supplemental Fig. S9) agrees with the value 4.89 predicted for the primary amino acid sequence by

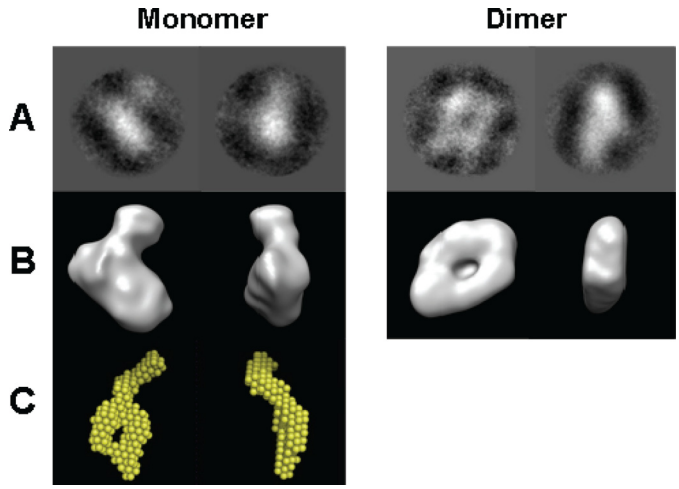

FIGURE 3. **Structures of the fibulin 5 monomer in the absence of Ca^{2+} and the dimer in the presence of Ca^{2+}.** *A*, selected representative class averages from EM single-particle image processing comparable with *B*, orthogonal views of the volume-rendered EM three-dimensional reconstructions. Thresholds were determined by matching theoretical standard hydrodynamic parameters calculated by Hydromic (42) for the reconstructions with experimentally measured parameters (Table 1). *C*, a "most probable" SAXS model for fibulin 5 is shown as touching spheres in orthogonal orientations.

Sednterp (37), which also predicts that each monomer has a charge of −28.7 at pH 7.3. Increasing the salt concentration further to 500 mM reduced the proportion of dimer, as is shown by Fig. 1*C*, where the peak at 14.5 ml is composed entirely of monomer. The equilibrium at 150 mM NaCl was shifted further toward the dimer on the addition of Ca^{2+} (Fig. 2*B* and supplemental Fig. S8).

EM Structures for Monomeric and Dimeric Full-length Fibulin 5—Negatively stained images were obtained for monomeric fibulin 5 in the absence of Ca^{2+} and dimeric fibulin 5 in the presence of Ca^{2+}, and three-dimensional reconstructions were calculated. The Hydromic (42) software determined thresholds for which the calculated theoretical standard hydrodynamic parameters of the EM structures matched those parameters determined by sedimentation velocity experiments (Table 1). Fig. 3*B* displays projections of the EM structures with the Hydromic-derived thresholds.

SAXS Solution Structure of Monomeric Full-length Fibulin 5—X-ray scattering measurements were made on a solution of monomeric fibulin 5 in the absence of Ca^{2+}. Aggregation was ruled out because the Guinier plot (supplemental Fig. S10*B*) was linear. The radius of gyration (R_g) was 4.20 ± 0.04 nm. The structure of fibulin 5 was determined *ab initio* by sequential application of the Gnom (32) and Gasbor (33) programs that provided good and coincident fits of the raw scattering data (supplemental Fig. S10*A*). Twenty separate simulations of Gasbor (33) were run, and the average three-dimensional structure (Fig. 3*C*) was calculated using the Damaver software (34). Theoretical sedimentation of this structure by Hydropro (43) gave an $s_{20,w}$ and an R_H that agreed with values derived from velocity sedimentation experiments (Table 1).

DISCUSSION

Fibulin 5 is a Ca^{2+}-binding protein of critical importance in the assembly of elastic fibers, and mutations in the fibulin gene cause cutis laxa (11–13) and have been implicated in age-related macular degeneration (14, 15). There are no high resolution structures for any of the fibulins, so knowledge of their structures is confined to comparisons with cbEGF-like domains for which high resolution structures exist (44). In the nonphysiological absence of Ca^{2+}, our compact SAXS and EM structures for monomeric fibulin 5 agree with but improve upon previous lower resolution EM images (26). The appearance of the hole in the SAXS structure (Fig. 3*C*) might be explained if the Fc module folds back along a linear series of cbEGF repeats. Our EM structure of dimeric fibulin 5 in the presence of Ca^{2+} suggests a head-to-tail arrangement of monomers. The dimerization of fragments that contain just the cbEGF domains suggest that intermolecular cbEGF interactions cause dimerization of full-length fibulin 5. It is likely that Ca^{2+} mediates these interactions. It has previously been shown that Ca^{2+} mediates contacts between identical human clotting factor IX cbEGFs in a crystal (45).

Fibulin 5 operates in the normal extracellular [Ca^{2+}] range 1.0–1.25 mM and in 135–145 mM NaCl (46). We found that the fibulin 5 dimer concentration is dominant in physiological solutions and is buffered strongly by NaCl and Ca^{2+} against changes in extracellular cation concentrations. A minimum dimer-dissociation constant of 0.86 μM was reached in a 150 mM NaCl solution on the addition of only 0.5 mM Ca^{2+}. The sensitivity of dimerization to Ca^{2+}, the presence of 0.6 mM Ca^{2+} in the media, and the acquisition of primarily monomeric fibulin 5 from Ni^{2+}-affinity and size-exclusion chromatographies performed in the absence of both Ca^{2+} and chelators (data not shown) suggest that dimers can dissociate. This is consistent with the picture of dynamic exchange between monomer and dimer populations drawn by the sedimentation data. Dissociation may explain why the maximum fraction of dimer is 0.7 rather than unity (supplemental Fig. S8), but it does not explain why it is independent of Ca^{2+} concentrations above 0.5 mM. The presence of low masses in the $c(M)$ distribution (supplemental Fig. S7*B*) suggests that higher order oligomers can also dissociate.

To date we have failed to crystallize fibulin 5, and this may be due to its flexibility and the [NaCl] and [Ca^{2+}] dependence of oligomerization. Except by size-exclusion chromatography, it is difficult to obtain a homogeneous preparation of one oligomeric form, and the salts contained in many crystallization conditions may only increase heterogeneity. Binding calcium protects some cbEGF-rich proteins against proteolytic degradation (47). For fibulin 5, any such effect could be augmented by dimerization reducing access to proteolytic cleavage sites.

The elastogenesis functions of fibulin 5 may be affected by its oligomerization. It is possible that the monomer or the dimer or both are "active" with regard to a function, but dimerization may provide a method for limiting interactions with binding partners. Binding studies should be reinterpreted in the light of equilibrium results presented here. For example, enhancement of the binding of fibulin 5 to tropoelastin by Ca^{2+} (10, 24) could result directly from Ca^{2+}-mediated binding or indirectly from Ca^{2+}-mediated conformational change or dimerization of fibulin 5. The experimental conditions (high salt in the absence of Ca^{2+}) in the work of Cirulis *et al.* (25) suggest that monomeric

fibulin 5 is responsible for elastin polypeptide self-assembly maturation slowing activity. It will be interesting to see how the Ca^{2+}-bound dimer affects the maturation of elastin assemblies.

Acknowledgments—We thank Adam Huffman (Bioinformatics), Paul Fullwood (DNA Sequencing), Dr. Patrick Bryant (Crystallography), and the EM Facility Staff from the Faculty of Life Sciences, and Dr. Nicoletta Bobola, Faculty of Medical and Human Sciences (University of Manchester, Manchester M13 9PL, United Kingdom); Dr. Manfred Roessle (Deutsches Elektronen-Synchrotron, Hamburg, Germany); and Dr. Rowan Orme (Keele University, Keele, Staffordshire ST5 5BG, United Kingdom).

REFERENCES

1. Argraves, W. S., Greene, L. M., Cooley, M. A., and Gallagher, W. M. (2003) *EMBO Rep.* **4,** 1127–1131
2. Chu, M. L., and Tsuda, T. (2004) *Birth Defects Res. C. Embryo. Today* **72,** 25–36
3. de Vega, S., Iwamoto, T., and Yamada, Y. (2009) *Cell. Mol. Life Sci.* **66,** 1890–1902
4. Timpl, R., Sasaki, T., Kostka, G., and Chu, M. L. (2003) *Nat. Rev. Mol. Cell Biol.* **4,** 479–489
5. Kowal, R. C., Richardson, J. A., Miano, J. M., and Olson, E. N. (1999) *Circ. Res.* **84,** 1166–1176
6. Nakamura, T., Ruiz-Lozano, P., Lindner, V., Yabe, D., Taniwaki, M., Furukawa, Y., Kobuke, K., Tashiro, K., Lu, Z., Andon, N. L., Schaub, R., Matsumori, A., Sasayama, S., Chien, K. R., and Honjo, T. (1999) *J. Biol. Chem.* **274,** 22476–22483
7. Kielty, C. M., Sherratt, M. J., and Shuttleworth, C. A. (2002) *J. Cell Sci.* **115,** 2817–2828
8. Bailey, A. J. (2001) *Mech. Ageing Dev.* **122,** 735–755
9. Nakamura, T., Lozano, P. R., Ikeda, Y., Iwanaga, Y., Hinek, A., Minamisawa, S., Cheng, C. F., Kobuke, K., Dalton, N., Takada, Y., Tashiro, K., Ross, Jr., J., Honjo, T., and Chien, K. R. (2002) *Nature* **415,** 171–175
10. Yanagisawa, H., Davis, E. C., Starcher, B. C., Ouchi, T., Yanagisawa, M., Richardson, J. A., and Olson, E. N. (2002) *Nature* **415,** 168–171
11. Claus, S., Fischer, J., Mégarbané, H., Mégarbané, A., Jobard, F., Debret, R., Peyrol, S., Saker, S., Devillers, M., Sommer, P., and Damour, O. (2008) *J. Invest. Dermatol.* **128,** 1442–1450
12. Loeys, B., Van Maldergem, L., Mortier, G., Coucke, P., Gerniers, S., Naeyaert, J. M., and De Paepe, A. (2002) *Hum. Mol. Genet.* **11,** 2113–2118
13. Markova, D., Zou, Y., Ringpfeil, F., Sasaki, T., Kostka, G., Timpl, R., Uitto, J., and Chu, M. L. (2003) *Am. J. Hum. Genet.* **72,** 998–1004
14. Lotery, A. J., Baas, D., Ridley, C., Jones, R. P., Klaver, C. C., Stone, E., Nakamura, T., Luff, A., Griffiths, H., Wang, T., Bergen, A. A., and Trump, D. (2006) *Hum. Mutat.* **27,** 568–574
15. Stone, E. M., Braun, T. A., Russell, S. R., Kuehn, M. H., Lotery, A. J., Moore, P. A., Eastman, C. G., Casavant, T. L., and Sheffield, V. C. (2004) *N. Engl. J. Med.* **351,** 346–353
16. Hirai, M., Ohbayashi, T., Horiguchi, M., Okawa, K., Hagiwara, A., Chien, K. R., Kita, T., and Nakamura, T. (2007) *J. Cell Biol.* **176,** 1061–1071
17. Freeman, L. J., Lomas, A., Hodson, N., Sherratt, M. J., Mellody, K. T., Weiss, A. S., Shuttleworth, A., and Kielty, C. M. (2005) *Biochem. J.* **388,** 1–5
18. Liu, X., Zhao, Y., Gao, J., Pawlyk, B., Starcher, B., Spencer, J. A., Yanagisawa, H., Zuo, J., and Li, T. (2004) *Nat. Genet.* **36,** 178–182
19. Hirai, M., Horiguchi, M., Ohbayashi, T., Kita, T., Chien, K. R., and Nakamura, T. (2007) *EMBO J.* **26,** 3283–3295
20. Zanetti, M., Braghetta, P., Sabatelli, P., Mura, I., Doliana, R., Colombatti, A., Volpin, D., Bonaldo, P., and Bressan, G. M. (2004) *Mol. Cell. Biol.* **24,** 638–650
21. Kapetanopoulos, A., Fresser, F., Millonig, G., Shaul, Y., Baier, G., and Utermann, G. (2002) *Mol. Genet. Genomics* **267,** 440–446
22. Nguyen, A. D., Itoh, S., Jeney, V., Yanagisawa, H., Fujimoto, M., Ushio-Fukai, M., and Fukai, T. (2004) *Circ. Res.* **95,** 1067–1074
23. Lomas, A. C., Mellody, K. T., Freeman, L. J., Bax, D. V., Shuttleworth, C. A., and Kielty, C. M. (2007) *Biochem. J.* **405,** 417–428
24. Wachi, H., Nonaka, R., Sato, F., Shibata-Sato, K., Ishida, M., Iketani, S., Maeda, I., Okamoto, K., Urban, Z., Onoue, S., and Seyama, Y. (2008) *J. Biochem.* **143,** 633–639
25. Cirulis, J. T., Bellingham, C. M., Davis, E. C., Hubmacher, D., Reinhardt, D. P., Mecham, R. P., and Keeley, F. W. (2008) *Biochemistry* **47,** 12601–12613
26. Kobayashi, N., Kostka, G., Garbe, J. H., Keene, D. R., Bächinger, H. P., Hanisch, F. G., Markova, D., Tsuda, T., Timpl, R., Chu, M. L., and Sasaki, T. (2007) *J. Biol. Chem.* **282,** 11805–11816
27. Golovanov, A. P., Hautbergue, G. M., Wilson, S. A., and Lian, L. Y. (2004) *J. Am. Chem. Soc.* **126,** 8933–8939
28. Ludtke, S. J., Baldwin, P. R., and Chiu, W. (1999) *J. Struct. Biol.* **128,** 82–97
29. van Heel, M., Harauz, G., Orlova, E. V., Schmidt, R., and Schatz, M. (1996) *J. Struct. Biol.* **116,** 17–24
30. Frank, J., Shimkin, B., and Dowse, H. (1981) *Ultramicroscopy* **6,** 343–357
31. Roessle, M. W., Klaering, R., Ristau, U., Robrahn, B., Jahn, D., Gehrmann, T., Konarev, P., Round, A., Fiedler, S., Hermes, C., and Svergun, D. (2007) *J. Appl. Crystallogr.* **40,** S190–S194
32. Semenyuk, A. V., and Svergun, D. I. (1991) *J. Appl. Crystallogr.* **24,** 537–540
33. Svergun, D. I., Petoukhov, M. V., and Koch, M. H. J. (2001) *Biophys. J.* **80,** 2946–2953
34. Volkov, V. V., and Svergun, D. I. (2003) *J. Appl. Crystallogr.* **36,** 860–864
35. Whitmore, L., and Wallace, B. A. (2004) *Nucleic Acids Res.* **32,** W668–W673
36. Compton, L. A., and Johnson, W. C., Jr. (1986) *Anal. Biochem.* **155,** 155–167
37. Hayes, D., Laue, T., and Philo, J. (1995) *Program Sednterp: Sedimentation Interpretation Program,* Alliance Protein Laboratories, Thousand Oaks, CA
38. Lewis, M. S., and Junghans, R. P. (2000) *Methods Enzymol.* **321,** 136–149
39. Schuck, P. (2000) *Biophys. J.* **78,** 1606–1619
40. Vistica, J., Dam, J., Balbo, A., Yikilmaz, E., Mariuzza, R. A., Rouault, T. A., and Schuck, P. (2004) *Anal. Biochem.* **326,** 234–256
41. Johnson, W. C., Jr. (1990) *Proteins Struct. Funct. Genet.* **7,** 205–214
42. de la Torre, J. G., Llorca, O., Carrascosa, J. L., and Valpuesta, J. M. (2001) *Eur. Biophys. J. Biophys. Lett.* **30,** 457–462
43. García De La Torre, J., Huertas, M. L., and Carrasco, B. (2000) *Biophys. J.* **78,** 719–730
44. Downing, A. K., Knott, V., Werner, J. M., Cardy, C. M., Campbell, I. D., and Handford, P. A. (1996) *Cell* **85,** 597–605
45. Rao, Z., Handford, P., Mayhew, M., Knott, V., Brownlee, G. G., and Stuart, D. (1995) *Cell* **82,** 131–141
46. Hope, R. A. (1993) *Oxford Handbook of Clinical Medicine* (Hope, R. A., Longmore, J. M., Hodgetts, T. J., and Ramrakha, T. S., eds) 3rd Ed., Oxford University Press, Oxford, UK
47. Reinhardt, D. P., Ono, R. N., and Sakai, L. Y. (1997) *J. Biol. Chem.* **272,** 1231–1236